Size-Dependent Electron-Electron Interactions in Metal Nanoparticles

C. Voisin, D. Christofilos, N. Del Fatti, and F. Vallée
Laboratoire d'Optique Quantique du CNRS, Ecole Polytechnique, 91128 Palaiseau cedex, France

B. Prével
Département de Physique des Matériaux, Université Lyon I, 69622 Villeurbanne cedex, France

E. Cottancin, J. Lermé, M. Pellarin, and M. Broyer
Laboratoire de Spectrométrie Ionique et Moléculaire, Université Lyon I, 69622 Villeurbanne cedex, France
(Received 28 April 2000)

The internal thermalization dynamics of the conduction electrons is investigated in silver nanoparticles with radius ranging from 13 to 1.6 nm using a femtosecond IR pump–UV probe absorption saturation technique. A sharp increase of the electron energy exchange rate is demonstrated for nanoparticles smaller than 5 nm. The results are consistent with electron-electron scattering acceleration due to surface induced reduction of the Coulomb interaction screening by the conduction and core electrons.

PACS numbers: 78.47.+p, 42.65.–k, 73.61.Tm

Reduction of the size of a material to a nanometric scale leads to drastic modifications of its physical properties that evolve from those of a solid to those of a few atom cluster. In metallic systems, conduction electron scattering processes play a key role in these properties and investigation of their alteration by the confinement is thus of both fundamental and technological interest [1]. Time resolved femtosecond techniques are powerful tools for studying electron interactions in bulk material and have been recently applied to metal nanoparticles [2–10] yielding information on electron-phonon [5–9] and electron-surface scattering [6,10]. The impact of confinement on electron-electron scattering, and on the correlated internal thermalization dynamics of the conduction electrons, has however not been addressed. We report here on the first investigation of the internal electron thermalization dynamics in small metal clusters. Measurements were performed using a two-color femtosecond absorption saturation technique in a model system formed by spherical silver particles embedded in a matrix. The results yield direct evidence for increase of the electron-electron interactions for sizes smaller than 5 nm.

The investigation technique is an extension of that used in noble metal films [11,12], and takes advantage of the sensitivity of the metal interband absorption on the energy distribution of the conduction electrons. This is first selectively perturbed by intraband (free electrons) absorption of a near infrared pulse, creating a strongly athermal distribution (dashed line in Fig. 1a, assuming instantaneous excitation). Electron-electron scattering subsequently redistributes the energy in the electron gas leading to a hot Fermi distribution, corresponding to an occupation number change Δf localized around the Fermi energy E_F (full line in Fig. 1a). Absorption around the interband transition threshold $\hbar\Omega_{\mathrm{ib}}$ being dominated by transitions from the full d bands to empty states around the Fermi surface it is very sensitive to Δf close to E_F and thus to the thermal or athermal character of the distribution.

A similar approach can be used in noble metal nanoparticles embedded in a transparent dielectric matrix, taking into account modification of the material optical properties by the dielectric confinement. For a low volume

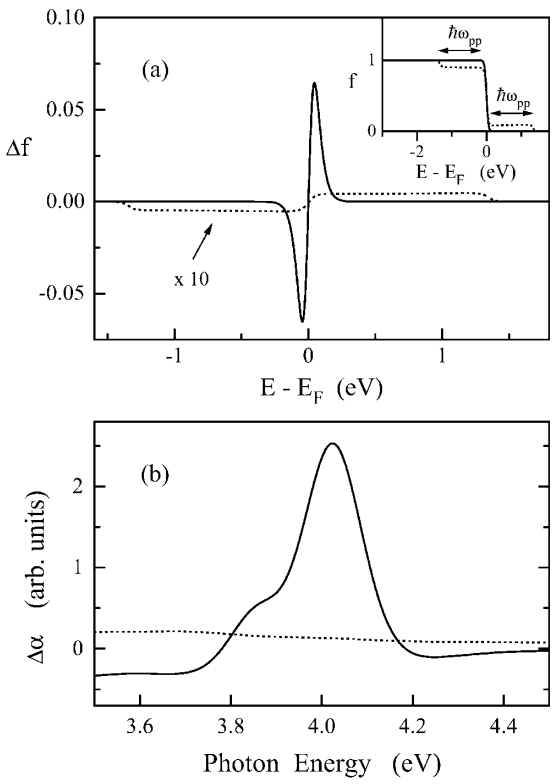

FIG. 1. (a) Change of the electron occupation number Δf around E_F for thermal (full line) and athermal (dashed line) distributions. The inset schematically shows the initial (full line) and perturbed (dashed line) electron distributions. ω_{pp} is the pump pulse frequency. (b) Corresponding absorption changes around the interband transition threshold computed for the $R = 3$ nm Ag particle sample for the thermal and athermal distributions (full and dashed lines, respectively).

 0031-9007/00/85(10)/2200(4)$15.00

fraction of small particles (with radius $R \ll \lambda$, where λ is the optical wavelength), the absorption coefficient of the composite material can be expressed in terms of the complex dielectric function of the metal nanoparticles $\epsilon(\omega) = \epsilon_1(\omega) + i\epsilon_2(\omega)$ [1]:

$$\alpha(\omega) = A \frac{\omega \epsilon_2(\omega)}{[\epsilon_1(\omega) + 2\epsilon_m]^2 + \epsilon_2^2(\omega)}, \qquad (1)$$

where A is a constant and ϵ_m the matrix dielectric constant. As compared to bulk metal, absorption is resonantly enhanced around the frequency, Ω_R, where the denominator is minimum, which is the condition for the surface plasmon resonance. Conversely to other noble metals, this takes place in silver away from the interband transitions ($\hbar\Omega_R \approx 3$ eV as compared to $\hbar\Omega_{\mathrm{ib}} \approx 4$ eV). Experiments were thus performed in silver nanoparticle samples where absorption modification in the interband transition region can be selectively studied.

The absorption change $\Delta\alpha$ induced by electron excitation reflects that of the metal particle dielectric function [Eq. (1)] and can be calculated by connecting $\Delta\epsilon$ to Δf [11–13]. Band structure changes being negligible for the investigated nanoparticle sizes ($R > 1.5$ nm) [1], this can be done using the bulk silver band structure model of Rosei [13]. The computed $\Delta\alpha$ spectra are shown in Fig. 1b for the athermal and thermal distribution changes of Fig. 1a (the two distributions correspond to the same injected energy). In the athermal case $\Delta\alpha$ exhibits a small amplitude with a broad structureless spectrum, in sharp contrast with that for the thermal situation. In particular, a strong increase of $\Delta\alpha$ when probing around 4 eV is predicted, reflecting the buildup of Δf close to E_F, and thus permitting one to follow the electron thermalization.

The near infrared and UV pulses necessary for the experiments were created using a femtosecond Ti:sapphire oscillator generating 25 fs frequency tunable pulses around 950 nm. The output of the laser was split into two parts, the first one being used as the pump beam. The UV probe pulses were generated by frequency tripling the second part. The typical UV average power was 10 μW with a pulse duration of 60 fs. The excitation process being nonresonant is weakly sensitive to the pump wavelength and probe photon energy dependent measurements can be performed by changing the operating wavelength of the oscillator. The two beams were sent in a standard pump-probe setup with mechanical chopping of the pump beam and lock-in detection of the probe beam transmission change ΔT (defined as the difference between the perturbed and unperturbed sample transmission). The reflectivity change being negligible, $\Delta T/T$ is directly proportional to the absorption change: $\Delta T/T = -\Delta\alpha L$, where L is the sample thickness.

Spherical silver nanoparticles embedded either in a $50BaO\text{-}50P_2O_5$ or in a Al_2O_3 matrix were investigated. The former samples were prepared by a fusion and heat treatment technique and the average particle radius R ranges from 2 to 13 nm [14]. The latter, with $1.5 \leq R \leq 2$ nm, were grown using low energy cluster beam deposition with codeposition of alumina [15].

The probe wavelength dependence of $-\Delta T/T$ measured around $\hbar\Omega_{\mathrm{ib}}$ in the $R = 3$ nm sample is shown in Fig. 2 for two pump-probe time delays: $t_D = 20$ and 400 fs. The measured spectral shapes are in good agreement with the computed ones for, respectively, athermal and thermal distributions (Fig. 1). In particular, a larger amplitude of $-\Delta T/T$ around $\hbar\omega_{\mathrm{pr}} \approx 4$ eV is observed for $t_D = 400$ fs than for $t_D = 20$ fs, yielding evidence for a delayed electron thermalization. Similar shapes were observed for all the investigated samples, confirming that band structure modifications are negligible for the investigated particle sizes and that the different samples are probed in similar conditions. The conduction electron thermalization dynamics can thus be compared for different particle sizes by monitoring the time dependent transmission change around 4 eV.

The time behaviors of $-\Delta T/T$ measured for $\hbar\omega_{\mathrm{pr}} \approx 3.95$ eV and $\hbar\omega_{\mathrm{pp}} \approx 1.32$ eV are plotted in Fig. 3 for $R = 1.6$, 3, and 12.1 nm, together with the pump-probe cross correlation. In all samples, $-\Delta T/T$ exhibits a delayed rise, with, for instance, a maximum amplitude at $t_D \approx 250$ fs for $R = 3$ nm demonstrating the existence of a non-Fermi distribution in metal nanoparticles on a few hundred femtosecond time scale. Furthermore, the observed rise time decreases with R yielding evidence for faster electron thermalization in small particles.

To be more quantitative, we have defined a characteristic internal thermalization time τ_{th} by fitting the measured signal assuming a monoexponential rise and using a phenomenological response function of the form

$$u(t) = H(t)[1 - \exp(-t/\tau_{\mathrm{th}})]\exp(-t/\tau_{\mathrm{ph}}), \qquad (2)$$

where $H(t)$ is the Heaviside function. The exponential decay of $u(t)$ with the time τ_{ph} stands for electron energy transfer to the lattice [10]. By convolving $u(t)$ with

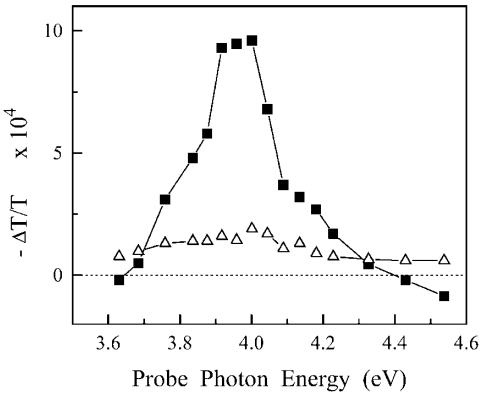

FIG. 2. Change of transmission $-\Delta T/T = \Delta\alpha L$ measured around the interband transition threshold for pump-probe delays of 20 fs (triangles) and 400 fs (squares) in the $R = 3$ nm Ag nanoparticle sample. The pump fluence is 180 μJ/cm^2.

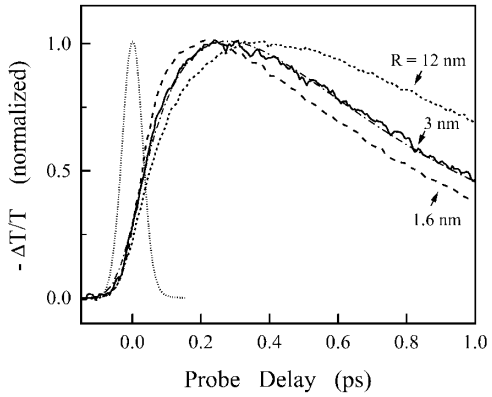

FIG. 3. Time behavior of the induced transmission change $-\Delta T/T$ measured for $\hbar\omega_{\mathrm{pr}} \approx 3.95$ eV and $\hbar\omega_{\mathrm{pp}} \approx 1.32$ eV in the $R = 12$ nm (dotted line), 3 nm (full line), and 1.6 nm (dashed line) Ag nanoparticle samples. The dash-dotted line is a fit for the $R = 3$ nm case using Eq. (2) and the short-dotted line the pump-probe cross correlation.

the pump-probe cross correlation, a good reproduction of the $\Delta T/T$ time behavior is obtained as shown in Fig. 3 for the $R = 3$ nm sample using $\tau_{\mathrm{th}} \approx 250$ fs. For $R \geq 5$ nm, τ_{th} is comparable to the one determined in a silver film using a similar technique ($\tau_{\mathrm{th}} \approx 350$ fs [12]). It strongly decreases for smaller sizes with, for instance, $\tau_{\mathrm{th}} \approx 160$ fs for $R = 1.6$ nm (Fig. 4). Comparable results were obtained for nanoparticles embedded either in the $50BaO\text{-}50P_2O_5$ or in the Al_2O_3 matrix (Fig. 4), showing that the observed τ_{th} variation is independent of the environment and sample preparation method.

The slow establishment of a Fermi-Dirac distribution in metal is a consequence of electron-electron (*e-e*) interaction reduction due to the many body effects and Pauli exclusion. This last effect leads to blocking of the final states for electron scattering and thus to a strong decrease of the probability of the *e-e* collisions around the Fermi energy. Since they are the slowest collision processes

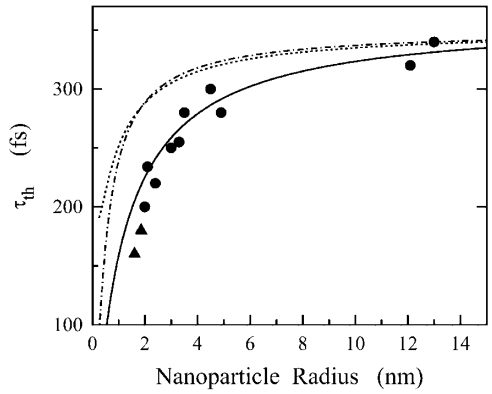

FIG. 4. Size dependence of the electron thermalization time τ_{th} for Ag nanoparticles in a $BaO\text{-}P_2O_5$ (dots) and Al_2O_3 (triangles) matrix. The full line shows the computed τ_{th} taking into account both the spillout and *d*-electron localization effects, and the dash-dotted and dotted lines their respective contributions.

involved in electron thermalization, they essentially determine τ_{th}. Consequently the thermalization dynamics is independent of the injected energy in the weak perturbation regime (i.e., induced electron temperature rises smaller than about 300 K) for which smearing of the electron distribution around E_F is small, but is perturbation dependent for larger energy injection [12]. To test a possible effect due to larger heating of the small particles, we have checked that our results are independent of both the pump fluence and the pump photon energy (using excitation either at the fundamental, $\hbar\omega_{\mathrm{pp}} \approx 1.32$ eV, or second harmonic, $\hbar\omega_{\mathrm{pp}} \approx 2.64$ eV, of the laser for the same probe $\hbar\omega_{\mathrm{pr}} \approx 3.95$ eV). This last point is important here since, on the average, less than one photon is absorbed per nanoparticle for small sizes and the minimum injected energy in a particle is thus set by $\hbar\omega_{\mathrm{pp}}$. The observed acceleration of the conduction electron thermalization can thus be ascribed to an intrinsic effect of the metal nanoparticles, i.e., confinement induced fastening of the electron energy exchanges.

Using the Fermi liquid theory, electron interactions can be described by a Coulomb potential screened by both the conduction and bound electrons (*d* electrons in noble metals). Because of the strong impact of the surfaces, the electron environment is different in a cluster as compared to the bulk metal. In particular, it was shown that the wave functions of the conduction electrons extend beyond the particle radius, leading to a reduction of their density n_e close to the surface (electron spillout [16]). Conversely, the *d*-electron wave functions are localized in the inner region of the particle leading to an incomplete embedding of the conduction electrons in the core electron background [17,18]. Both effects lead to less efficient screening of the Coulomb interactions close to a surface [19,20] and are thus expected to increase the effective *e-e* scattering rate in small nanoparticles.

With the measured τ_{th} being similar in metal films and large clusters (Fig. 4) we have estimated the influence of these surface effects by introducing them as corrections. Assuming static screening, one can show that in the bulk material the dependence of the scattering rate of an electron out of its state on the electron density and core electron screening is given by [21]

$$\gamma_e \propto n_e^{-5/6} \epsilon_d^{-1/2}, \tag{3}$$

where ϵ_d is the *d*-electron contribution to the static metal dielectric function. For a weak perturbation, τ_{th} is directly related to γ_e^{-1}. As a first approximation, we have thus estimated the global scattering rate in the particle assuming γ_e to have a similar expression as in the bulk [Eq. (3)], with position dependent n_e and ϵ_d, and spatially averaging it taking into account the particle electron density. Although this local approach is a crude approximation, it is partly justified by the short screening distance of the Coulomb interaction (on a length of the order of the inverse of the Thomas-Fermi wave vector, ~ 1 Å in metals).

The spatial variations of ϵ_d and n_e in silver clusters were previously modeled to analyze the size dependence of the surface plasmon resonance frequency [18] and we have used the same approach here. The d-electron surface exclusion effect is described using a phenomenological two-region dielectric model, where screening by the d electrons is effective only in a core sphere of radius $R_c = R - c$ with $c = 3.5$ a.u. (i.e., $\epsilon_d = \epsilon_d^{\text{bulk}}$ inside the core sphere and $\epsilon_d = 1$ outside). The smooth spatial variation of n_e around the surface is calculated using the jellium dielectric sphere model [18]. The estimated R dependence of τ_{th} reproduces well the experimental one, indicating important contributions from both the spillout and d-electron localization effects (Fig. 4). No parameter is used here, the absolute value of the calculated τ_{th} being set by imposing its large particle ($R \geq 25$ nm) value to be identical to the bulk one. With the n_e spatial profile close to the surface being almost independent of R for the investigated sizes, the calculated τ_{th} size dependence essentially reflects the increasing relative number of electron in the perturbed surface layer (about 25% of the electrons are out of the R_c radius core sphere for $R = 2$ nm), i.e., the increasing influence of the surface in small clusters.

Although a good reproduction of the data is obtained, a systematic deviation is observed for small sizes ($R \leq 2$ nm). The above model, based on a simple extension of the bulk calculations with phenomenologic inclusion of the surface effects using a local approach, clearly overlooks specific features of the confined materials. In particular, the e-e scattering rate has been derived using the bulk electron wave functions and includes momentum conservation. This is relaxed in the confined system, due to, classically, electron scattering off the surfaces and is expected to lead to further size-dependent modifications of the e-e interactions. A more correct description requires nonlocal calculations of the e-e scattering and many body effects in a nanoparticle using the confined electrons wave functions and is out of the scope of this paper.

In conclusion, using a two-color femtosecond absorption saturation technique, we have performed the first investigation of the internal electron thermalization dynamics in metal clusters. Experiments were performed in a model system formed by silver nanoparticles embedded in a dielectric matrix where establisment of an electron temperature can be selectively studied. This is shown to take place on a few hundred femtosecond time scale, comparable to that in metal films for large particles but strongly accelerated for smaller ones ($R \leq 5$ nm). The similar results, obtained for different matrices and electron excitation conditions, permit one to ascribe the observed thermalization fastening to increase of electron-electron scattering in small particles. The size dependence of the thermalization time is in good agreement with a simple model which phenomenologically introduces surface induced reduction of the Coulomb interaction screening due to the spillout and d-electron wave function localization effects. Additional theoretical works are, however, clearly necessary to model electron-electron interactions in metal particles, and, in particular, the transition from the bulk material to small size clusters.

The authors wish to thank A. Nakamura for helpful discussions and S. Omi for providing the BaO-P_2O_5 embedded silver nanoparticles.

[1] U. Kreibig and M. Vollmer, *Optical Properties of Metal Clusters* (Springer-Verlag, Berlin, 1995).
[2] T. Tokizaki, A. Nakamura, S. Kavelo, K. Uchida, S. Omi, H. Tanji, and Y. Asahara, Appl. Phys. Lett. **65**, 941 (1994).
[3] J. Y. Bigot, J. C. Merle, O. Cregut, and A. Daunois, Phys. Rev. Lett. **75**, 4702 (1995).
[4] M. Perner, P. Bost, U. Lemmer, G. von Plessen, J. Feldmann, U. Becker, M. Mennig, M. Schmitt, and H. Schmidt, Phys. Rev. Lett. **78**, 2192 (1997).
[5] M. Nisoli, S. Stagira, S. De Silvestri, A. Stella, P. Tognini, P. Cheyssac, and R. Kofman, Phys. Rev. Lett. **78**, 3575 (1997).
[6] N. Del Fatti, C. Flytzanis, and F. Vallée, Appl. Phys. B **68**, 433 (1999).
[7] V. Halté, J. Y. Bigot, B. Palpant, M. Broyer, B. Prével, and A. Pérez, Appl. Phys. Lett. **75**, 3799 (1999).
[8] S. Link and M. A. El-Sayed, J. Phys. Chem. B **103**, 8410 (1999), and references therein.
[9] J. H. Hodak, A. Henglein, and G. V. Hartland, J. Chem. Phys. **111**, 8613 (1999).
[10] N. Del Fatti, F. Vallée, C. Flytzanis, Y. Hamanaka, and A. Nakamura, Chem. Phys. **251**, 215 (2000).
[11] C. K. Sun, F. Vallée, L. H. Acioli, E. P. Ippen, and J. G. Fujimoto, Phys. Rev. B **50**, 15 337 (1994).
[12] N. Del Fatti, C. Voisin, M. Achermann, S. Tzortzakis, D. Christofilos, and F. Vallée, Phys. Rev. B **61**, 16 956 (2000).
[13] R. Rosei, Phys. Rev. B **10**, 474 (1974).
[14] K. Uchida, S. Kaneko, S. Omi, C. Hata, H. Tanji, Y. Asahara, A. J. Ikushima, T. Tokisaki, and A. Nakamura, J. Opt. Soc. Am B **11**, 1236 (1994).
[15] B. Palpant, B. Prével, J. Lermé, E. Cottancin, M. Pellarin, M. Treilleux, A. Perez, J. L. Vialle, and M. Broyer, Phys. Rev. B **57**, 1963 (1998).
[16] W. Ekardt, Phys. Rev. B **29**, 1558 (1984).
[17] A. Liebsch, Phys. Rev. B **48**, 11 317 (1993).
[18] J. Lermé, B. Palpant, B. Prével, M. Pellarin, M. Treilleux, J. L. Vialle, A. Perez, and M. Broyer, Phys. Rev. Lett. **80**, 5105 (1998).
[19] N. Nilius, N. Ernst, and H.-J. Freund, Phys. Rev. Lett. **84**, 3994 (2000).
[20] J. Kliewer, R. Berndt, E. V. Chulkov, V. M. Silkin, P. M. Echenique, and S. Crampin, Science **288**, 1399 (2000).
[21] D. Pines and P. Nozières, *The Theory of Quantum Liquids* (Benjamin, New York, 1966).